Separation Science and Technology
Publication details, including instructions for authors and subscription information:
http://www.informaworld.com/smpp/title~content=t713708471

Adsorption of Carbon Dioxide onto Activated Carbon and Nitrogen-Enriched Activated Carbon: Surface Changes, Equilibrium, and Modeling of Fixed-Bed Adsorption

Tirzhá L. P. Dantas[ab]; Suélen M. Amorim[a]; Francisco Murilo T. Luna[c]; Ivanildo J. Silva Jr.[c]; Diana C. S. de Azevedo[c]; Alírio E. Rodrigues[b]; Regina F. P. M. Moreira[a]
[a] Department of Chemical and Food Engineering, Federal University of Santa Catarina, Campus Universitário, Trindade, Florianópolis, Brazil [b] Department of Chemical Engineering, Faculty of Engineering, University of Porto, Porto, Portugal [c] Department of Chemical Engineering, Federal University of Ceará, Fortaleza, CE, Brazil

Online publication date: 07 January 2010

To cite this Article Dantas, Tirzhá L. P. , Amorim, Suélen M. , Luna, Francisco Murilo T. , Silva Jr., Ivanildo J. , de Azevedo, Diana C. S. , Rodrigues, Alírio E. and Moreira, Regina F. P. M.(2010) 'Adsorption of Carbon Dioxide onto Activated Carbon and Nitrogen-Enriched Activated Carbon: Surface Changes, Equilibrium, and Modeling of Fixed-Bed Adsorption', Separation Science and Technology, 45: 1, 73 — 84
To link to this Article: DOI: 10.1080/01496390903401762
URL: http://dx.doi.org/10.1080/01496390903401762

Separation Science and Technology, 45: 73–84, 2010

ISSN: 0149-6395 print/1520-5754 online
DOI: 10.1080/01496390903401762

Taylor & Francis
Taylor & Francis Group

Adsorption of Carbon Dioxide onto Activated Carbon and Nitrogen-Enriched Activated Carbon: Surface Changes, Equilibrium, and Modeling of Fixed-Bed Adsorption

Tirzhá L. P. Dantas,[1,3] Suélen M. Amorim,[1] Francisco Murilo T. Luna,[2] Ivanildo J. Silva Jr.,[2] Diana C. S. de Azevedo,[2] Alírio E. Rodrigues,[3] and Regina F. P. M. Moreira[1]

[1]*Department of Chemical and Food Engineering, Federal University of Santa Catarina, Campus Universitário, Trindade, Florianópolis, Brazil*
[2]*Department of Chemical Engineering, Federal University of Ceará, Fortaleza, CE, Brazil*
[3]*Department of Chemical Engineering, Faculty of Engineering, University of Porto, Porto, Portugal*

It has been reported that the CO_2 adsorption capacity of the N-enriched activated carbon can increase or decrease. In this study a commercial activated carbon was functionalized with 3-chloropropylamine hydrochloride and its adsorption characteristics in a fixed-bed column were investigated. The N-enriched activated carbon presented lower BET surface area than the original activated carbon suggesting that the nitrogen incorporation partially blocks the access of N_2 to the small pores. Although the surface basicity has increased it is not accomplished by an increase of the capacity of the adsorption of the N-enriched activated carbon. The breakthrough curves in a fixed bed column were obtained at different temperatures (301 K, 323 K, 373 K, and 423 K) and a total pressure of 1.01 bar using CO_2 diluted in helium at two feed concentrations—10% and 20% (v/v). A model based on the Linear Driving Force (LDF) model for mass transfer was used to estimate the overall mass transfer coefficient and reproduced the breakthrough curves satisfactorily.

Keywords adsorption; carbon dioxide; activated carbon; functionalization

INTRODUCTION

According to the IPCC (Intergovernmental Panel on Climate Change), some direct and indirect measurements have confirmed that the carbon dioxide concentration in the atmosphere has grown globally by around 100 ppm (36%) in the last 250 years: from 275–285 ppm in the pre-industrial age to around 380 ppm in 2005.

Most of the CO_2 released into the atmosphere results from fossil fuel burning and it is identified as one of the major contributors to global warming and climate changes currently observed around the world.

There are 3 (three) possibilities available for reducing carbon dioxide emission (1).

i. reducing the energy demand;
ii. exchanging the current energy matrices for renewable energy, clean fuels, or nuclear energy and
iii. carbon dioxide capture.

A reduction in the energy demand is impracticable since industrial development has left us highly dependent on energy and fossil fuels represent approximately 85% of the current global energy consumption. The increase in the CO_2 concentration in the atmosphere could be controlled with alternative energy sources; however, it is known that it will take a certain amount of time for technologies that use renewable energies and clean fuels to be consolidated and for the production costs to fall.

The pathways of CO_2 separation through pre-combustion decarbonation (that is, CO_2 capture after the gasification process and before the combustion stage), O_2/CO_2 recycle combustion (using O_2 instead of air combustor), or post-combustion separation (CO_2 capture from the exhaustion gases) can be readily carried out using known technologies and processes.

However, existing technologies still present a series of problems related to application in post-combustion separation, including the great volume of the exhaustion gases and the cost-benefit ratio (2). Thus, the goal of reducing carbon dioxide emissions on an industrial scale requires the development of low-cost capture methods. Adsorption is an excellent method of post-combustion separation and has been shown to be an efficient alternative to separation since adsorbents have a high adsorption capacity, high selectivity, good mechanical properties, ease of regeneration

Received 9 October 2008; accepted 7 August 2009.
Address correspondence to Alírio E. Rodrigues, Laboratory of Separation and Reaction Engineering (LSRE), Department of Chemical Engineering, Faculty of Engineering, University of Porto, Rua Dr. Roberto Frias s/n, Porto 4200-465, Portugal. Tel.: +351 22 508 1671;; Fax: +351 22 508 1674 E-mail: arodrig@fe.up.pt

and they remain stable over repeated adsorption/desorption cycles (3).

Activated carbon is a suitable adsorbent and its CO_2 adsorption characteristics are dependent on its surface area and chemical surface characteristics. The surface chemistry of activated carbon is determined by the amount and type of heteroatom, for example oxygen, nitrogen, etc. These heteroatoms exist in the acid, basic, or neutral form of organic functional groups (4). Therefore, the adsorption capacity of activated carbon for carbon dioxide is a function of its pore structure and the properties of the surface chemistry (5).

Nitrogen in a carbonaceous matrix can cause an increase in the basic group number and therefore modify the load distribution at the surface of the solid. Some authors have reported the positive effect of nitrogen incorporation on the activated carbon adsorption of H_2S (6,7) and also SO_x and NO_x(8). Recently, some authors have investigated the modification of CO_2 adsorption capacity on activated carbon (5,9,10,11,12) or other supports (13,14,15) through the enrichment of the surface with nitrogen functionalities.

Immobilized amines have demonstrated characteristics similar to those currently used typical absorption processes in liquid phase, with the advantage that the solids can be handled easily and reduce the problem of corrosion in the equipment (2).

In this study, an amine was evaluated as a potential source of basic sites for CO_2 capture. A commercial activated carbon was enriched with nitrogen by addition of 3-chloropropylamine hydrochloride ($C_3H_8ClN.HCl$) and its CO_2 adsorption capacity and other characteristics were investigated. The solids adsorbents (commercial activated carbon and nitrogen-enriched activated carbon) were characterized in terms of the apparent surface area, micropore volume, and pore size distribution. The surface changes caused by amine enrichment were investigated by TGA and FTIR analysis. The adsorption of carbon dioxide on the adsorbents packed in a fixed-bed was studied. The experimental breakthrough curves were obtained using two different fractions of carbon dioxide diluted in an inert gas (helium) at four different temperatures: 301 K, 323 K, 373 K, and 423 K. A model based on the Linear Driving Force (LDF) approximation for mass transfer, taking into account the energy balance, was used to describe the adsorption kinetics of carbon dioxide.

EXPERIMENTAL SECTION

The gases used in this studied were provided by Air Liquide S.A (Portugal) or by White Martins Ltda (Brazil).

Carbon Dioxide N48 was provided by Air Liquide S.A (Portugal). This gas was used in the determination of the carbon dioxide adsorption equilibrium on activated carbon.

Helium (99.995%), carbon dioxide (99.998%), and standard mixtures (10% and 20% CO_2/He v/v) were provided by White Martins Ltd.

Nitrogen-Enriched Activated Carbon Preparation

The commercial activated carbon used was Norit R2030 (Norit, Netherlands) which was selected due to its high adsorption capacity for CO_2 (16). The nitrogen-enriched activated carbon, denoted as CPHCl, was prepared in a way similar way to that as described by Gray et al. (13), mixing 10 g of activated carbon with 500 mL of 10^{-1} M 3-chloropropylamine hydrochloride solution (melting point: 421 K–423 K). The mixture was kept under constant stirring, at ambient temperature for 5 hours. The CPHCl adsorbent was then left to dry for 12 hours in an oven at 378 K.

Characterization of the Adsorbents

The elemental analysis was carried out using CHNS EA1100 equipment (CE Instruments, Italy).

The textural characterization was performed by the nitrogen sorption measurements at 77 K, using an automatic sorptometer, Autosorb 1C (Quantachome, USA). The N_2 surface area obtained from the BET equation within the 0.001–0.2 relative pressure range was calculated because, despite its controversial interpretation for activated carbons, this parameter provides a value that can be useful when comparing the characteristics of different activated carbons.

Thermogravimetric experiments were carried out with a TGA-50 thermogravimetric analyzer (Shimadzu, Japan) in the temperature range of 303–1173, at a heating rate of 10 K/min under nitrogen flow.

Fourier transform infrared (FTIR) spectroscopy was used to qualitatively identify the chemical functionality of activated carbon. To obtain the observable adsorption spectra, the solids were grounded to an average diameter of ca. 0.5 μm. The transmission spectra of the samples were recorded using KBr pellets containing 0.1% of carbon. The pellets were 12.7 mm in diameter and ca. 1 mm thick and were prepared in a manual hydraulic press set at 10 ton. The spectra were measured from 4000 to 400 cm^{-1} and recorded on a 16PC FTIR spectrometer (Perkin Elmer, USA).

Adsorption Equilibrium Isotherms

The equilibrium of CO_2 adsorption on commercial activated carbon was measured at different temperatures of 301 K, 323 K, 373 K, and 423 K using the static method in a Rubotherm magnetic suspension microbalance (Bochum, Germany) up to approximately 5 bar. The equilibrium of CO_2 adsorption on CPHCl was measured at different temperatures of 298 K, 323 K, 373 K, and 423 K by the volumetric method, in an automatic sorptometer,

TABLE 1
Physical properties of the fixed-bed

Bed Lengh L, m	0.171
Bed Diameter d_C, m	0.022
Bed Weight W, kg	0.0351
Voidage adsorbent bed, ε	0.52
Column wall specific heat, $C_{p,w}$	440 J kg^{-1}K^{-1}
Wall density, ρ_w	7828 kg m^{-3}

Autosorb 1C (Quantachome, USA), up to approximately 1 bar. Before the CO_2 adsorption measurements, the solid samples were pre-treated for 12 hours at 423 K under vacuum. This temperature ensures that the amine is homogeneously tethered to the solid surface without devolatilize or decompose it.

Fixed Bed CO_2 Adsorption Dynamics–Breakthrough Curves

The experimental breakthrough curves were obtained by passing the gas mixture of CO_2 diluted in helium through the packed column with the adsorbent: commercial activated carbon or CPHCl. The solid adsorbent was pre-treated by passing helium at a flow rate of 30 mL/min min and at 423 K for 2 hours. These breakthrough curves were obtained at 301 K, 323 K, 373 K, and 423 K. The total gas flow rate was 30 mL/min at 1 bar total pressure. Two different fractions, y_F, of CO_2 diluted in helium were used: 0.1 and 0.2 (v/v). The physical properties of the fixed-bed are given in Table 1.

The reversibility of the adsorption was studied in desorption experiments by passing pure helium through the packed column at a total flow rate of 30 mL/min.

The column was located inside a furnace with controlled temperature. The flow of gas was controlled by a mass flow unit (Matheson, USA). A gas chromatographic model CG35 (CG Instrumentos Científicos, Brazil) equipped with a Porapak-N packed column (Cromacon, Brazil) and with a thermal conductivity detector (TCD) was used to monitor the carbon dioxide concentration at the bed exit, using helium as the reference gas. At regular time's interval, 1 mL of the gas at the end of the column was taken, using a gas tight syringe and immediately analyzed by gas chromography.

The experimental system (column and furnace) was considered adiabatic because it was isolated with a layer of 0.10 m of fiber glass and with a refractory material.

DESCRIPTION OF MODEL FOR CO_2 ADSORPTION IN THE FIXED-BED

The model used to describe the fixed-bed dynamics is derived from the mass balance, taking into account the energy balance, with the axially dispersed plug flow model and the mass transfer rate represented by a Linear Driving Force (LDF) model. The LDF model is frequently used for this purpose because it is analytically simple and physically consistent.

Farooq and Ruthven (17) reported a comparison between one and two-dimensional models for the adsorption in a fixed bed, providing a simple approximate means of estimating the spread to be expected in the breakthrough curve for a given degree of nonisothermality, expressed in terms of a dimensionless radial conductivity parameter. They concluded that in adiabatic conditions, the radial temperature profile becomes flat and the one-dimensional model is suitable to describe the dynamics of adsorption in a fixed bed (17). The global mass balance was described by the axial dispersed plug flow model Eq. (1) (18).

$$-D_L\frac{\partial^2 C}{\partial z^2}+\frac{\partial(vC)}{\partial z}+\frac{\partial C}{\partial t}+\left(\frac{1-\varepsilon}{\varepsilon}\right)\frac{\partial \bar{q}}{\partial t}=0 \qquad (1)$$

where D_L is the axial dispersion, ε is the voidage of the adsorbent bed and v is the interstitial velocity. The feed consists of a small concentration of a single adsorbable component and the frictional pressure drop through the bed is negligible, thus, the linear velocity may be considered constant.

The rate of mass transfer to the particle was described by the linear driving force (Eq. 2). According to this approximation, the partial differential mass balance equation in the particle is replaced by a much simpler ordinary differential equation, which states that the uptake rate of CO_2 is proportional to the difference between the surface concentration and the average concentration within the particle.

$$\frac{\partial \bar{q}}{\partial t}=K_L(q-\bar{q}) \qquad (2)$$

where K_L is the LDF global mass transfer coefficient and q is the adsorbed equilibrium concentration, i.e., q = f(C) given by the adsorption equilibrium isotherm.

The energy balance in the fluid phase gives the variation of the gas temperature with the time (1). The heat balance was described by Eq. (3) (18).

$$\begin{aligned}-\lambda.\frac{\partial^2 T_g}{\partial z^2}+C_g\frac{\partial(vT_g)}{\partial z}+C_g\frac{\partial T_g}{\partial t}+\left(\frac{1-\varepsilon}{\varepsilon}\right)C_s\frac{\partial T_s}{\partial t}\\ =\left(\frac{1-\varepsilon}{\varepsilon}\right)(-\Delta H)\frac{\partial \bar{q}}{\partial t}-\frac{4h_w}{\varepsilon d_c}(T_g-T_w)\end{aligned} \qquad (3)$$

where λ is the thermal axial dispersion coefficient, C_g and C_s are the specific heat values for gas and solid phases, respectively, $(-\Delta H)$ is the isosteric heat adsorption, h_w is the internal convective heat coefficient between the gas and the wall, and d_c is the bed diameter.

The rate of heat transfer to the particle may be written as:

$$C_s \frac{\partial T_s}{\partial t} = \frac{6h_f}{d_p}(T_g - T_s) + (-\Delta H)\frac{\partial \bar{q}}{\partial t} \quad (4)$$

where h_f is the film heat transfer coefficient, and d_p is the particle diameter.

For the column wall, the energy balance for an adiabatic system can be expressed by:

$$\rho_w C_{p,w} \frac{\partial T_w}{\partial t} = \alpha_w h_w (T_g - T_w) \quad (5)$$

where ρ_w is the column wall density, $C_{p,w}$ is the column wall specific heat, and α_w is the ratio of the internal surface area to the volume of the column wall (19).

The value of the gas phase viscosity was estimated using the Wilke equation and the molecular diffusivities were calculated with the Chapman-Enskong equation (20).

The LDF global mass transfer coefficient considers all of the resistances to the mass transfer, i.e., intra- and extra-particle resistances. The value of the LDF global mass transfer coefficient was estimated using the expression proposed by Farooq and Ruthven (21) which considers film resistance, and macropore and micropore resistances:

$$\frac{1}{K_L} = \frac{r_p q_o}{3k_f C_o} + \frac{r_p^2 q_o}{15\varepsilon_p D_e C_o} + \frac{r_c^2}{15D_c} \quad (6)$$

where r_p is the particle radius, k_f the external mass transfer coefficient, q_0 the value of q at equilibrium with C_o (adsorbate concentration in the feed at feed temperature T_o and expressed in suitable units), ε_P the particle porosity, r_c the radius of activated carbon crystal, and D_c is the micropore diffusivity. The micropore diffusivity values were those reported by Cavenati and coworkers (19) since the micropore distribution of the adsorbents are similar to those of carbon molecular sieves (19,22).

The mass and heat transport parameters were estimated according to correlations reported in the literature (18,20,23,24,25). The correlations used to evaluate the mass and heat transport parameters are summarized in Table 2. The value of the mean pore radius (r_o) was 1.23 nm for commercial activated carbon and 1.54 nm for CPHCl, estimated through the nitrogen adsorption isotherm.

Tortuosity factor (τ) values of 2.2 and 1.8 for activated carbon and CPHCl, respectively, were assumed and the particle porosity of activated carbon and CPHCl are 0.47 and 0.37.

The mathematical model was solved using the commercial software gPROMS (Process System Enterprise Limited, UK) which uses the orthogonal collocation method on finite elements for resolution. The bed was divided into six sections with three collocation points for each element of the adsorption bed.

TABLE 2
Correlations used for estimation of mass and heat parameters

Bosanquet Equation	$\frac{1}{D_e} = \tau\left(\frac{1}{D_m} + \frac{1}{D_K}\right)$
Knudsen diffusion	$D_K = 9700 r_o \sqrt{\frac{T}{M_w}}$
Axial mass dispersion	$Pe = 0.508\mathrm{Re}^{0.020}\frac{L}{d_p}$; $Pe = \frac{uL}{D_L}$; $\mathrm{Re} = \frac{\rho_g u d_p}{\mu_g}$
Axial heat dispersion	$\frac{\lambda}{k_g} = 10 + 0.5\ \mathrm{Pr}\ \mathrm{Re}; \mathrm{Pr} = \frac{C_g \mu_g}{k_g}$
Internal convective heat coefficient	$\frac{h_w d_c}{k_g} = 12.5 + 0.048\mathrm{Re}$
Film mass transfer	$Sh = 1.09\ \mathrm{Re}^{0.27} Sc^{1/3}$; $Sc = \frac{\mu_g}{\rho_g D_m}$; $Sh = \frac{k_f d_p}{D_m}$
Film heat transfer	$Nu = 2.0 + 1.1\ \mathrm{Re}^{0.6}\ \mathrm{Pr}^{1/3}$; $Nu = \frac{h_f d_p}{k_g}$

RESULTS AND DISCUSSION

Characterization of the Adsorbent

The nitrogen sorption isotherms for the commercial activated carbon and for the CPHCl are shown in Fig. 1. The hysteresis loop is narrow, the adsorption and desorption branches are almost the same, indicating that both adsorbents are microporous. This kind of loop is designated type H4 hysteresis in the IUPAC classification and is usually found for solids consisting of aggregates or agglomerates of particles forming slit-shaped pores (26).

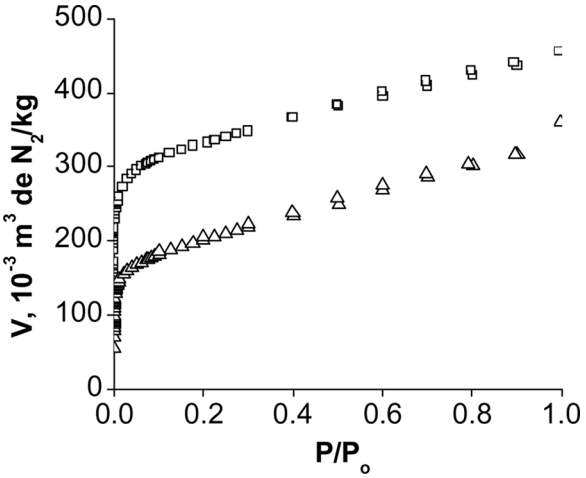

FIG. 1. Nitrogen sorption isotherms at 77 K: □ commercial activated carbon and △ CPHCl.

TABLE 3
Textural properties of the adsorbents studied

Adsorbent	Commercial activated carbon	CPHCl
S_{BET}, m^2/g	1053.0	664.6
S_{micro}, m^2/g	1343.0	753.0
V_{micro}, cm^3/g	0.0972	0.0388
N_2 Micropore Capacity, kg/kg	300	155
N_2 Total Capacity, kg/kg	370	260
Particle density $\rho_p.10^3$, kg/m^3	1.14	
Particle diameter d_p 10^3, m	3.8	
Adsorbent specific heat, J/kg.K	880	

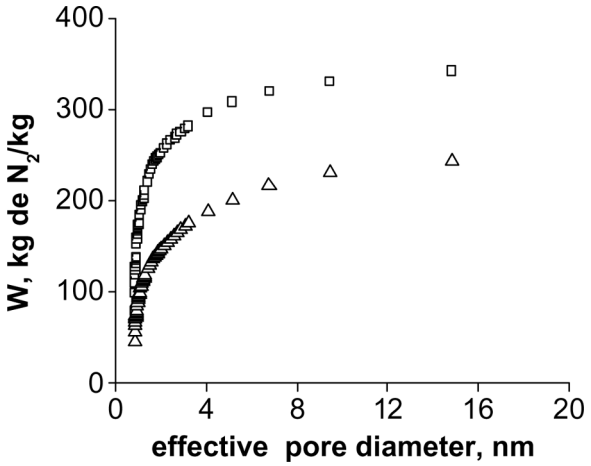

FIG. 2. Cumulative nitrogen adsorbed as a function of pore diameter calculated with the HK method from the N_2 sorption isotherms at 77 K: □ commercial activated carbon and △ CPHCl.

Table 3 summarizes the physical characterization obtained from the nitrogen sorption isotherm and mercury intrusion. The apparent surface area (S_{BET}) was evaluated using the BET equation (27), micropore area (S_{micro}) was calculated according to the DR method (28) and the micropore volume (V_{micro}) was determined by the t-method (29).

Modifications with nitrogen-containing species may also result in changes in the porous structure (11), as can be observed in the N_2 adsorption isotherms shown in Fig. 1. The CPHCl had a lower BET area when compared to the commercial activated carbon. The micropores volume of the CPHCl decreases considerably compared with the commercial activated carbon, suggesting that the nitrogen incorporation partially blocks the access of N_2 to the small pores.

The hysteresis loop of the N_2 adsorption isotherm occurs, for both adsorbents, at relative pressure closes to $P/Po = 0.4$. Below this pressure the pore filling mechanism is the so-called micropore filling, for which no hysteresis occurs. When the nitrogen pressures exceeds $P/Po = 0.4$, the mesopores are filled by means of capillary condensation (29). The micropore capacity, in terms of N_2, for the two adsorbents was taken from the hysteresis pressure (30,31), as seen in Table 4. For the calculations, the density

TABLE 4
Chemical characteristics of the adsorbents studied

Adsorbent	Commercial activated carbon	CPHCl
C	86.2	70.2
H	1.3	2.0
N	0.9	1.4
N/C. 10^2	1	2

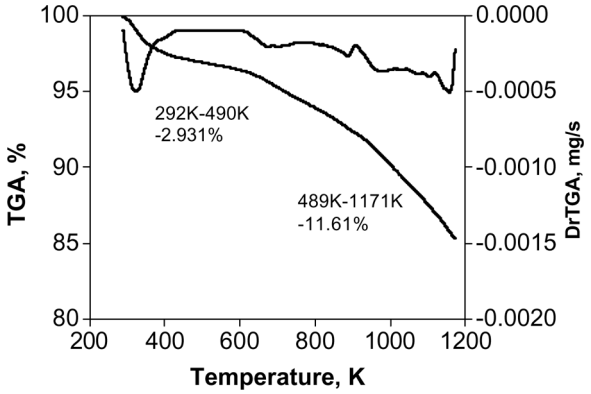

FIG. 3. TGA and DrTGA curves for commercial activated carbon.

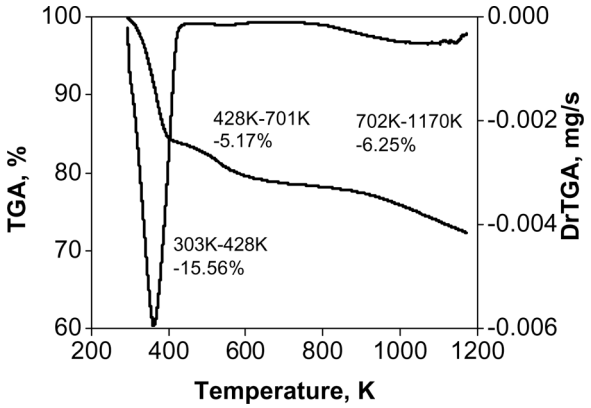

FIG. 4. TGA and DrTGA curves for CPHCl.

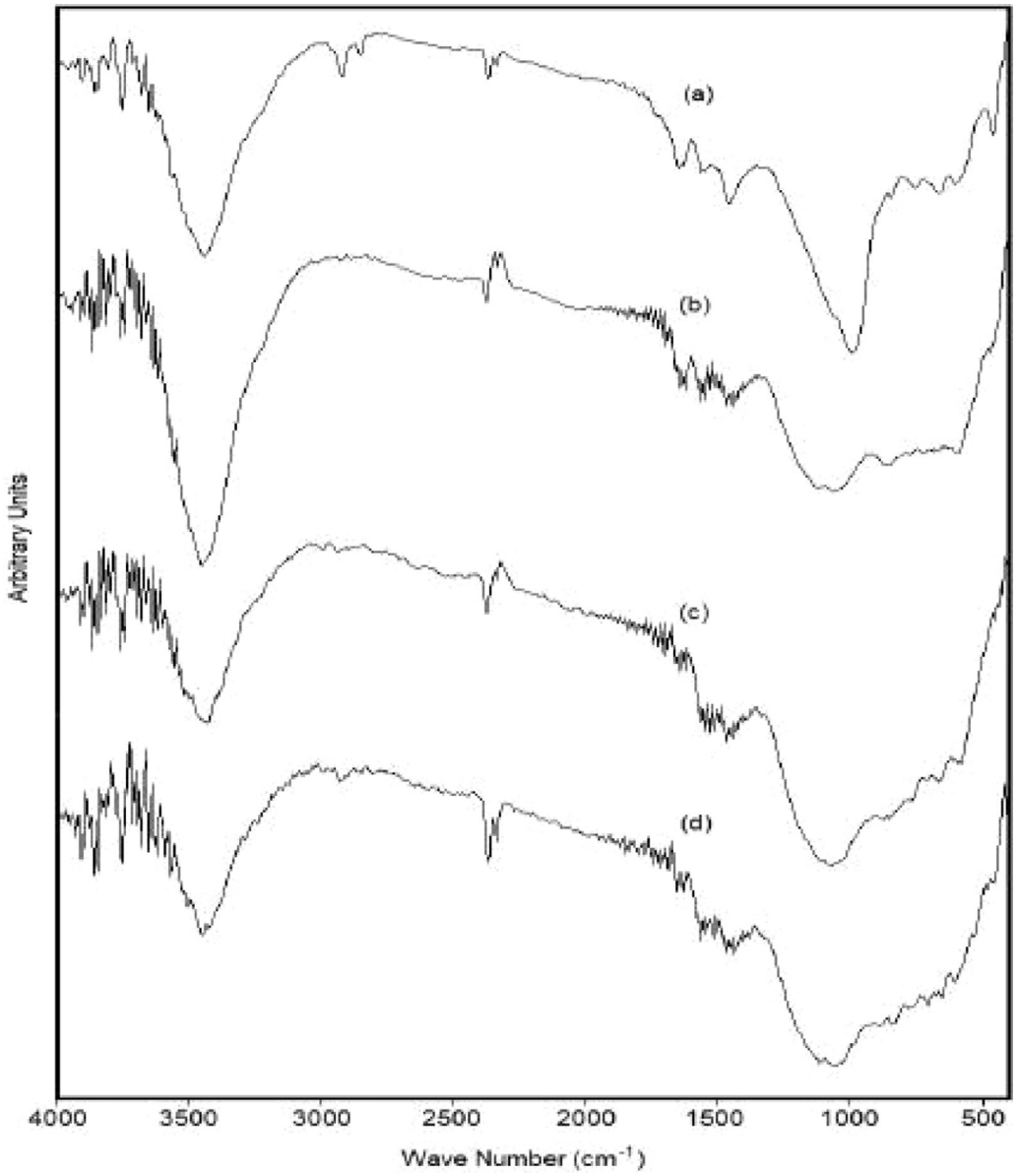

FIG. 5. FTIR spectra of (a) commercial activated carbon; (b) CPHCl; (c) CPHCl after pre-treatment and CO_2 adsorption at 301 K and (d) CPHCl after pre-treatment and CO_2 adsorption at 423 K.

of adsorbed nitrogen was approximated with its liquid density at 77 K (0.808 kg/m^3).

The effective micropore size distribution, for both adsorbents, was calculated using the HK method (32). The accumulated amount of N_2 adsorbed as a function of pore size is shown in Fig. 2 for the commercially activated carbon and for the CPHCl. From Fig. 2, it is evident that the great majority of the pores shown for the two adsorbents are micropores. Micropores have a diameter of less then 2 nm. However, the great microporosity of the activated carbon is evidenced by the fact that about 70% of its total capacity, in terms of N_2, is found to be in the micropores. However, for the CPHCl, approximately 52% of its total capacity is present in the micropores.

The chemical characteristics of the adsorbents are given in Table 4. As expected, the adsorbent CPHCl has the greater nitrogen content and an N/C atomic ratio which is twice that of the commercial activated carbon.

Figures 3 and 4 show the weight loss (TG) and the derivative thermogravimetric (DrTG) curves obtained for the commercial activated carbon and for the nitrogen-enriched activated carbon −CPHCL.

For the commercial activated carbon, the first range of thermal decomposition presents a little weight loss which

is due to release of the moisture. Further mass loss at temperature above 490 K is due to the release of the volatile matter which is consistent with the volatile matter content of the activated carbon, as measured by the ultimate analysis (33).

The CPHCl adsorbent had a mass loss at 303–428 K which is typical for phase changes, due to the melting of the amine and due to release of the moisture. The subsequent temperatures give the same total weight loss due to the volatiles.

The FTIR spectra of commercial activated carbon and CPHCl are shown in Fig. 5.

In the FTIR spectra the band of O-H stretching vibrations (3600–3100 cm^{-1}) was due to surface hydroxyl groups and chemisorbed water. The asymmetry of this band at lower wave numbers indicates the presence of strong hydrogen bonds.

It has been suggested that primary amine can react with the activated carbon surface, forming surface complexes with the presence of NH_2 surface groups (13). Bands were presence at 3365 and 1607 cm^{-1}, ascribed to asymmetric stretching (νNH_2) and NH_2 deformation, respectively, and at 3303 cm^{-1}. However, the CPHCl spectrum shows that these bands may be overlapped by the OH stretching band (3600–3100 cm^{-1}) and by the aromatic ring bands and double bond (C=C) vibrations (1650–1500 cm^{-1}) (34). The same pattern is observed for CPHCl after CO_2 adsorption at 301 K and 423 K, indicating that there is no difference in the adsorption behavior.

Carbon Dioxide Adsorption Equilibrium Isotherms

The CO_2 adsorption equilibrium isotherms for commercial activated carbon and CPHCl are shown in the Figs. 6 and 7, respectively.

The CO_2 adsorption equilibrium for commercial activated carbon was described using the Toth model (35) Eq. (7).

$$q = \frac{q_m K_{eq} P}{[1 + (K_{eq} P)^n]^{1/n}} \tag{7}$$

where q_m is the maximum adsorbed concentration, i.e., the monolayer capacity; K_{eq} is the equilibrium adsorption constant and n is the heterogeneity parameter of the solid.

The CO_2 adsorption equilibrium for CPHCl was described according to the linear model (Eq. 8). The dependence of K_{eq} or K_p on the temperature was described according to the Van't Hoff equation.

$$q = K_p P \tag{8}$$

where K_p is the Henry's Law constant for the adsorption equilibrium.

Table 5 gives the parameters used in this study for Toth fitting. It is worth mentioning that the commercial activated carbon used in this studied has a high CO_2 adsorption capacity in comparison with other adsorbents reported in literature (36,37).

Table 6 gives the Henry's Law constants for the adsorption equilibrium on CPHCl, at the different temperatures studied, the pre-exponencial factor and heat of adsorption. Table 7 shows the Henry's constants for the adsorption equilibrium on commercial activated carbon that was fitted at low pressure.

It should be noted, however, that the commercial activated carbon has higher Henry's Law constant indicating that this solid has a greater carbon dioxide adsorption capacity.

The nature of the N functionality is very important because it can affect the basicity of the solid surface (38).

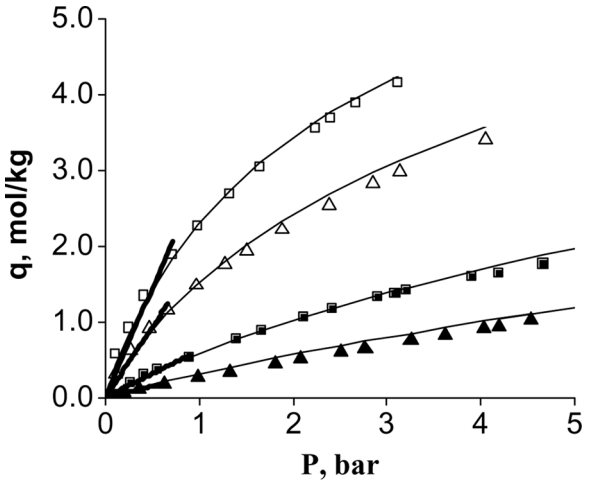

FIG. 6. Adsorption equilibrium isotherms for carbon dioxide on commercial activate carbon at different temperatures: □ 301 K; △ 323 K; ■, 373 K and ▲ 423 K. Solid lines: Toth Model. Bold line: linear model.

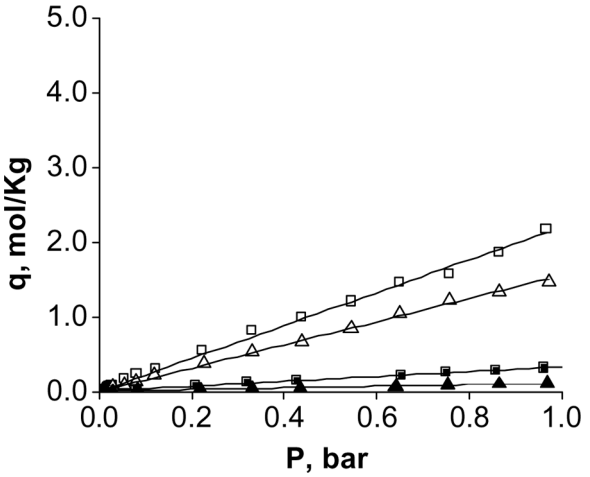

FIG. 7. Adsorption equilibrium isotherms for carbon dioxide on CPHCl at different temperatures: □ 298 K; △ 323 K; ■, 373 K and ▲ 423 K. Solid lines: Linear Model.

TABLE 5
Parameters of adsorption isotherm for carbon dioxide on different adsorbents and parameters used for fitting of the Toth model

q_m, mol/kg	n	K_o 10^5, bar^{-1}	$-\Delta H$, kJ/mol
10.05	0.678	7.62	21.84

Comparing a primary amine with a secondary amine of the same carbon number, the basic character increases due to the increase in the inductive effect caused by the alkyl groups (39). Some authors have reported that although there is a reduction in the BET superficial area which is caused by the partial blockage of the lesser pores, as also observed in this paper, the enrichment of the carbonaceous materials with nitrogen tends to increase the adsorption capacity for CO_2(11). However, there is no consensus about this issue because sorbents with the high amounts of nitrogen do not have the high CO_2 adsorption capacity reported in recent publications by Arenillas and coworkers (11) and Pevida et al. (40). In the present study, we show a decrease in the CO_2 adsorption capacity of CPHCl in comparison with non-functionalized activated carbon.

The decrease in the CO_2 adsorption capacity is not related to the destruction of basic sites in the CPHCl, as shown in the FTIR studies (Fig. 5). In fact, Drage et al. (12) have reported that only an activation temperature higher than 873 K can destroy the basic sites in the adsorbents.

Modeling the Breakthrough Curves

As previously mentioned, a set of experiments was performed changing the temperature and the feed concentration of the carbon dioxide to determine the breakthrough curves. The experimental conditions and the LDF global

TABLE 6
Henry's Law constants for the adsorption equilibrium on commercial activated carbon and CPHCl at different temperatures

	Commercial activated carbon	CPHCl	
T, K	K_p, moles/kg. bar	K_p, moles/kg. bar	$-\Delta H$, kJ/mol
301–298	2.89	2.16	20.25
323	1.86	1.55	
373	0.62	0.32	
423	0.29	0.11	

TABLE 7
Experimental Conditions and LDF global mass transfer coefficient for CO_2 adsorption on the commercial activated carbon and CPHCl

				K_L, s^{-1}	
Run	y_F	T, K	Pe	Commercial activated carbon	CPHCl
1	0.1	301	21.75	0.0027	0.0041
2		323	21.69	0.0043	0.0063
3		373	21.59	0.0125	0.0259
4		423	21.49	0.0259	0.0719
5	0.2	301	21.91	0.0027	0.0041
6		323	21.85	0.0043	0.0063
7		373	21.75	0.0125	0.0259
8		423	21.65	0.0259	0.0719

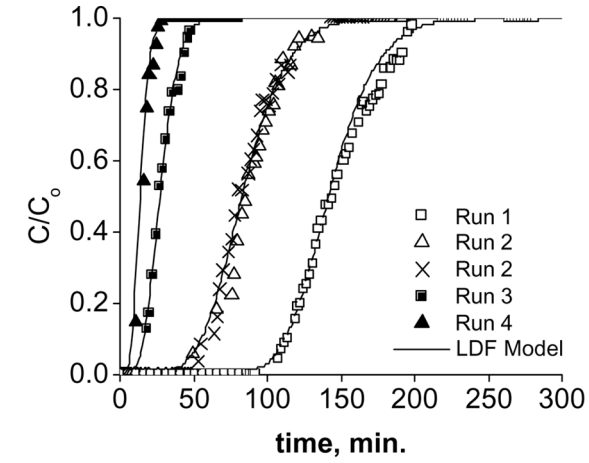

(a)

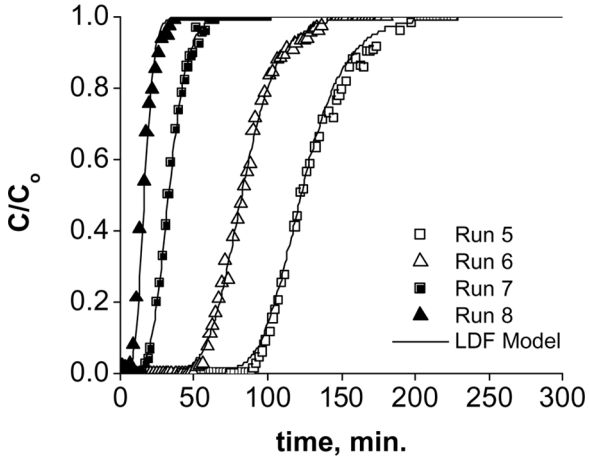

(b)

FIG. 8. Breakthrough curves for the CO_2 adsorption on commercial activated carbon. Symbols: experimental data; Lines: LDF model. (a) Runs 1 to 4 and (b) runs 5 to 8.

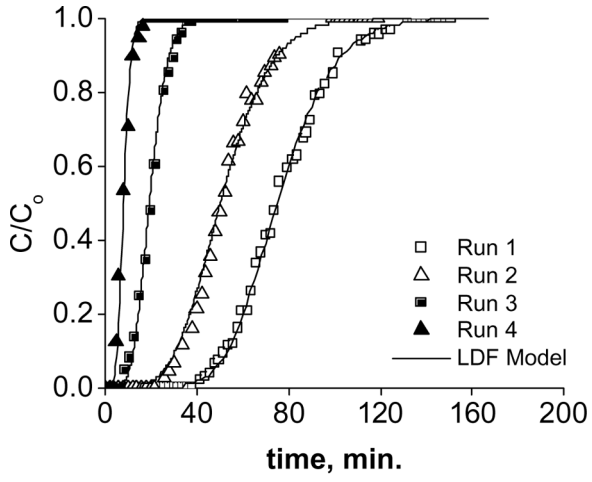

(a)

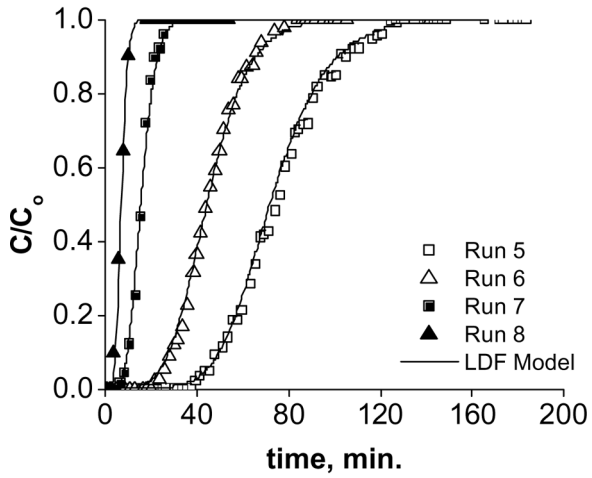

(b)

FIG. 9. Breakthrough curves for the CO_2 adsorption on CPHCl. Symbols: experimental data. Lines: LDF model. (a) Runs 1 to 4 and (b) runs 5 to 8.

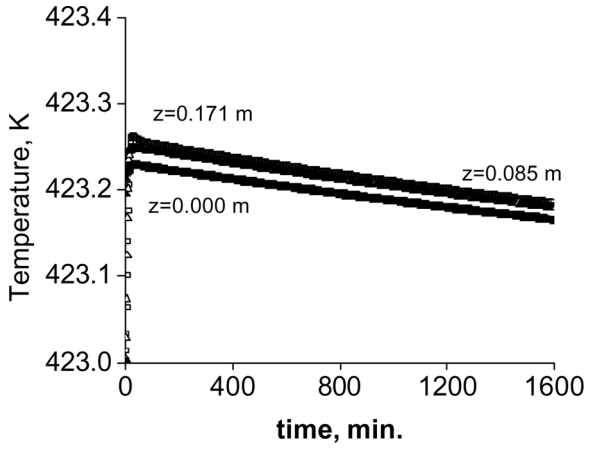

(a)

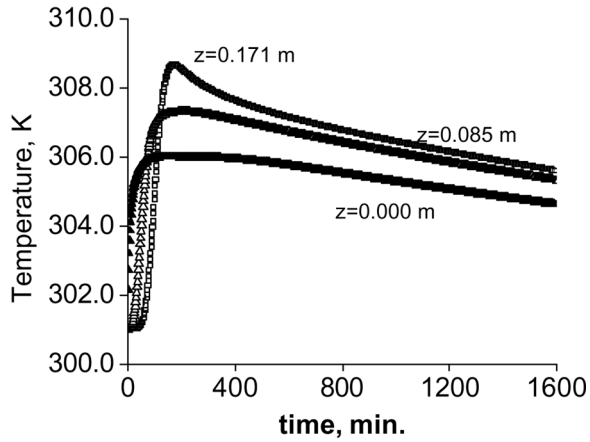

(b)

FIG. 10. Temperature profile for the carbon dioxide adsorption on commercial activated carbon. Conditions: (a) run 4 and (b) run 5. □ z = 0.171 m; △ z = 0.085 m and ▲ z = 0.000 m.

mass transfer coefficient calculated from Eq. (5) for the adsorption of carbon dioxide on commercial activated carbon and CPHCl are shown in Table 7.

Figure 8 shows a comparison between the experimental and theoretical curves obtained for the CO_2 adsorption on commercial activated carbon, using different molar fractions of CO_2. It is observed that, in the case of the mass balance, the model reproduces the experimental data for the different feed concentration and temperatures reasonably well. For any of the feed concentration, the amount of CO_2 adsorption decreases as the temperature increases, causing a shift on the breakthrough curves, since the adsorption is exothermic.

Figure 9 shows a comparison between the experimental and theoretical curves obtained for the CO_2 adsorption on CPHCl, using different molar fractions of CO_2. It is observed that the model reproduces adequately the experimental data for the different feed concentrations and temperatures.

The global mass transfer coefficient for CO_2 adsorption on CPHCl in the fixed bed is higher than that for the adsorption on activated carbon (Table 7) which was to be expected because the CPHCl is an adsorbent with less micropores and smaller CO_2 adsorption capacity than the commercial activated carbon. This makes the importance of the external to the internal mass transfer resistance (Eq. (5)) greater in the case of CPHCl than commercial activated carbon.

A sensitivity analysis was performed to determine the importance of the external and internal mass transfer resistances and it was observed that the simulated curves changed only when the resistance was decreased. Thus, it can be concluded that external mass transfer resistance is not

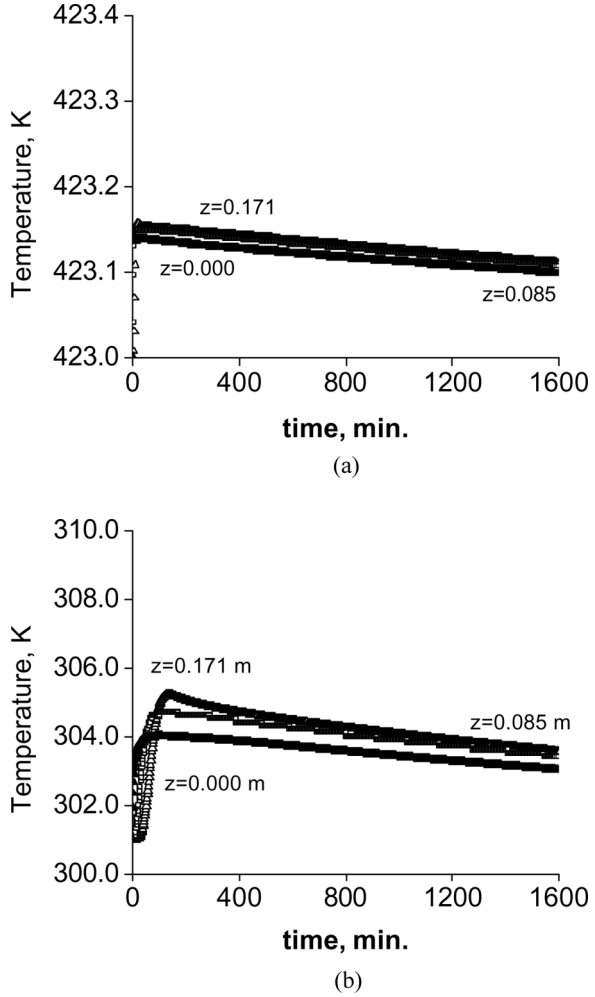

FIG. 11. Temperature profile for the carbon dioxide adsorption on CPHCl. Conditions: (a) run 4 and (b) run 5. □ z = 0.171 m; △ z = 0.085 m and ▲ z = 0.000 m.

important in the studied system, i.e., the intrinsic characteristics of the carbon materials is a determining factor in CO_2 adsorption and is of greater importance than the bed properties. Moreover, the intraparticle diffusion in the pores is predominant and the external mass transfer resistance can be neglected for all practical purposes (41).

Figures 10 and 11 show the simulated temperature profile for the carbon dioxide adsorption on commercial activated carbon and CPHCl, respectively, under experimental conditions of 423 K and feed CO_2 fraction of 0.1 (run 4) and for 301 K and feed CO_2 fraction of 0.2 (run 5).

In Figs. 10a and 11a, the temperature peak occurs below 1 K for activated carbon and CPHCl. However, at high CO_2 inlet concentration and low temperature (Figs. 10b and 11b), the temperature peaks is almost 8 K and 5 K, for activated carbon and CPHCl, respectively. This is due to exothermic adsorption and heat effects must be considered during adsorption. The adsorption can be considered isothermally only for low CO_2 concentration at the inlet of the column ($y_F < 0.1$) and/or at high temperatures (Figs. 10a and 10b). Moreover, as the commercial activated carbon and the CPHCl have about the same heat of adsorption, but distinct adsorptive capacities, it is also possible to conclude that a higher adsorption capacity leads to a higher temperature peak, since the adsorption is an exothermic phenomenon.

CONCLUSIONS

Carbon dioxide adsorption on a commercial activated carbon and on a nitrogen-enriched activated carbon packed in a fixed bed was studied. The adsorption equilibrium data for carbon dioxide on the commercial activated carbon were fitted well using the Toth model equation, whereas for carbon dioxide adsorption on the CPHCl a linear isotherm was considered.

There are many factors that influence CO_2 capture, some of them are physical and some chemical. Textural properties are important for any adsorption processes but, in the case of CO_2 capture, the surface chemistry is a particularly important factor. The enrichment of activated carbon with nitrogen using amine 3-chloropropylamine hydrochloride blocked some pores of the activated carbon. The increase in the surface basicity was not sufficient to counteract the decrease in the BET superficial area since a reduction in the CO_2 adsorption was observed.

A model using the LDF approximation for the mass transfer, taking into account the energy balance, described the breakthrough curves of carbon dioxide adequately. The LDF global mass transfer coefficient for the adsorption of CO_2 on activated carbon is smaller than that for the CPHCl. Since part of the micropores of the activated carbon are blocked by the incorporation of the amine in the CPHCl, probably only the largest pores would be filled by the CO_2, causing a decrease on the capacity of the adsorption and an increase on the adsorption rate.

NOTATION

C	concentration of the adsorbate, mol m^{-3}
C_o	concentration of the adsorbate in the feed, mol m^{-3}
C_g	specific heat for gas phase, J kg^{-1} K^{-1}
C_s	specific heat for solid phase, J kg^{-1} K^{-1}
$C_{p,w}$	column wall specific heat, J kg^{-1} K^{-1}
d_C	bed diameter, m
d_p	particle diameter, m
D_c	micropore diffusivity, m^2 s^{-1}
D_e	effective diffusivity, m^2 s^{-1}
D_L	axial dispersion coefficient, m^2 s^{-1}
D_m	molecular diffusivity, m^2 s^{-1}
D_K	Knudsen diffusivity, m^2 s^{-1}
h_f	film heat transfer coefficient, W m^{-2} K^{-1}

h_w	internal convective heat coefficient between the gas and the wall, W m^{-2} K^{-1}
k_f	external mass transfer coefficient, m^2 s^{-1}
k_g	gas thermal conductivity, W m^{-1} K^{-1}
K_{eq}	Toth constant for adsorption equilibrium, bar^{-1}
K_L	LDF global mass transfer coefficient, s^{-1}
K_o	Toth constant for adsorption equilibrium at the limit $T \rightarrow \infty$ bar^{-1}
K_p	Henry's Law constant for adsorption equilibrium, mol kg^{-1} bar^{-1}
L	bed length, m
M_w	molecular weight, kg/mol
n	Toth heterogeneity parameter of the solid.
Nu	Nusselt number
P	pressure, bar
Pe	Peclet number
Pr	Prandtl number
q	adsorbed concentration in equilibrium with the gas phase, mol kg^{-1}
q_0	value of q at equilibrium with C_o at T_o, mol m^{-3}
q_m	maximum adsorbed concentration, mol kg^{-1}
$\bar{q}$	average adsorbed concentration, mol kg^{-1}
r_p	particle radius, m
r_o	mean pore radius, m
r_c	crystal radius, m
Re	Reynolds number
S_{BET}	surface area calculated according to BET isotherm, m^2 g^{-1}
$S_{micro,}$	micropore area calculated according to DR method, m^2 g^{-1}
Sc	Schmidt number
Sh	Sherwood number
t	time, s
T	temperature, K
u	superficial velocity, m s^{-1}
v	interstitial velocity, m s^{-1}
$V_{micro,}$	micropore volume, cm^3 g^{-1}
Z	axial coordinate along the bed, m
W	bed weight, kg

Greek letters

$(-\Delta H)$	isosteric heat adsorption, J mol^{-1}
ε	Voidage of adsorbent bed
ε_P	particle porosity
λ	thermal axial dispersion coefficient, W m^{-1} K^{-1}
μ_g	gas viscosity, $N.sm^{-1}$
ρ_g	gas density, kg m^{-3}
ρ_p	particle density kg m^{-3}
ρ_w	wall density kg m^{-3}
τ	tortuosity

ACKNOWLEDGMENT

The authors would like to thank the financial support from Capes/Brazil.

REFERENCES

1. Grimston, M.C.; Fouquet, R.; Vorst, R. Van der.; Pearson, P.; Leach, M. (2001) The European and global potential of carbon dioxide sequestration in tackling climate change. *Climate Policy*, *1*: 155.
2. Plaza, M.G.; Pevida, C.; Arenillas, A.; Rubiera, F.; Pis, J.J. (2007) CO_2 capture by adsorption with nitrogen enriched carbons. *Fuels*, *86* (14): 2204.
3. Yong, Z.; Mata, V.; Rodrigues, A.E. (2002) Adsorption of carbon dioxide at high temperature–a review. *Sep. Purif. Technol.*, *26* (2–3): 195.
4. Moreno-Castila, C.; Carrasco-Marín, F.; Mueden, A. (1997) The creation of acid carbon surfaces by treatment $(NH_4)_2S_2O_2$. *Carbon*, *35* (10–11): 1619.
5. Maroto-Valer, M.M.; Tang, Z.; Zhang, Y. (2005) CO_2 capture by activated and impregnated anthracites. *Fuel Process. Technol.*, *86* (14–15): 1487–1502.
6. Adib, F.; Bagreev, A.; Bandosz, T.J. (2000) Adsorption/Oxidation of hydrogen sulfide on nitrogen-containing activated carbon. *Langmuir*, *16* (4): 1980.
7. Bagreev, A.; Menendez, J.A.; Dukhno, I.; Tarasenko, Y.; Bandosz, T.J. (2004) Bituminous coal-based activated carbons modified with nitrogen as adsorbents of hydrogen sulfide. *Carbon*, *42* (3): 469.
8. Mochida, I.; Koraia, Y.; Shirahama, M.; Kawano, S.; Hada, T.; Seo, Y.; Yoshikawa, M.; Yasutake, A. (2000) Removal of SO_x and NO_x over activated carbon fibers. *Carbon*, *38* (2): 227.
9. Przepiórski, J.; Skrodzewicz, M.; Morawsk, A.W. (2004) High temperature ammonia treatment of activated carbon for enhancement of CO_2 adsorption. *Appl. Surf. Sci.*, *225* (1–4): 235.
10. Arenillas, A.; Drage, T.C.; Smith, K.M.; Snape, C.E. (2005) CO_2 removal potential of carbons prepared by co-pyrolysis of sugar and nitrogen containing compounds. *J. Anal. Appl. Pyrolysis*, *74* (1–2): 298.
11. Arenillas, A.; Rubiera, F.; Parra, J.B.; Ania, C.O.; Pis, J.J. (2005) Surface modification of low costs carbons for their application in the environmental protection. *Appl. Surf. Sci.*, *252* (3): 619.
12. Drage, T.C.; Arenillas, A.; Smith, K.M.; Pevida, C.; Piipo, S.; Snape, C.E. (2007) Preparation of carbon dioxide adsorbents from the chemical activation of urea-formaldehyde and melamine-formaldehyde resins. *Fuel*, *86* (1–2): 22.
13. Gray, M.L.; Soong, Y.; Champagne, K.J.; Baltrus, J.P.; Stevens, Jr, R.W.; Toochinda, P.; Chuang, S.S.C. (2004) CO_2 capture by amine-enriched fly ash carbon sorbents. *Sep. Purif. Technol.*, *35* (1): 31.
14. Arenillas, A.; Smith, K.M.; Drage, T.C., Snape, C.E. (2005) CO_2 capture using fly ash-derived carbon materials. *Fuel*, *84* (17): 2204.
15. Gray, M.L.; Soong, Y.; Champagne, K.J.; Pennline, H.; Baltrus, J.P.; Stevens, Jr, R.W.; Khatri, R.; Chuang, S.S.C.; Filburn, T. (2005) Improved immobilized carbon dioxide capture sorbents. *Fuel Process. Technol.*, *86* (14–15): 1449.
16. Dantas, T.L.P.; Rezende, R.V.P.; Rodrigues, A.E., Moreira, R.F.P.M. (2008) Adsorção de CO_2 e N_2 sobre carvão ativado e zeólita 13X: Isotermas de Equilíbrio através de medidas gravimétricas. In: 7° Encontro Brasileiro sobre Adsorção- 1° Simpósio Sul-Americano sobre Ciência e Tecnologia de Adsorção (in Portuguese).
17. Farooq, S.; Ruthven, D.M. (1990) Heat effects in adsorption column dynamics. 1. Comparison of one and two-dimensional models. *Ind. Eng. Chem. Res.*, *29*: 1084.
18. Ruthven, D.M. (1984) *Principles of Adsorption and Adsorption Processes*; Wiley: New York.
19. Cavenatti, S.; Grande, C.A.; Rodrigues, A.E. (2006) Separation of $CH_4/CO_2/N_2$ mixtures by layered pressure swing adsorption for upgrade of natural gas. *Chem. Eng. Sci.*, *61* (12): 3893.
20. Bird, R.B.; Stewart, W.E.; Lightfoot, E.H. (1960) *Transport Phenomena*; Wiley: New York.

21. Farooq, S.; Ruthven, D.M. (1990) Heat effects in adsorption column dynamics. 2. Experimental validation of the one-dimensional model. *Ind. Eng. Chem. Res.*, *29*: 1084.
22. Vinu, A.; Hartmann, M. (2005) Characterization and microporosity analysis of mesoporous carbon molecular sieves by nitrogen and organics adsorption. *Catal. Today*, *102–103*: 189.
23. Incropera, F.P.; De Witt, D.P. (1996) *Fundamentals of Heat and Mass Transfer*; Wiley: New York.
24. Leitão, A.; Rodrigues, A.E. (1995) The simulation of solid-liquid adsorption in activated carbon columns using estimates of intraparticle kinetic parameters obtained from continuous stirred tank reactor experiments. *Chem. Eng. J.*, *58*: 239.
25. Seguin, D.; Montillet, A.; Brunjail, D. Comiti, J. (1996) Liquid-solid mass transfer in packed beds of variously shaped particles at low Reynolds numbers: experiments and model. *Chem. Eng. J.*, *63* (1): 1.
26. Leofanti, G.; Padovan, M.; Tozzola, G.; Venturelli, B. (1998) Surface area and pore texture of catalysts. *Catal. Today*, *41* (1–3): 207.
27. Brunauer, S.; Emmett, P.H.; Teller, E. (1938) Adsorption of gases in multimolecular layers. *J. Am. Chem. Soc.*, *60* (2): 309.
28. Dubinin, M.M.; Radushkevich, L.V. (1947) *Proc. Acad. Sci. Phys. Chem. Sec. USSR*, *55*: 331.
29. De Boer, J.H.; Lippens, B.C.; Lippens, B.G.; Broekhoff, J.C.P.; Van den Heuvel, A.; Osinga, Th.J. (1966) The T-curve of multimolecular N_2-adsorption. *J. Colloid Interface Sic.*, *21* (4): 405.
30. Do, D.D. (1998) *Adsorption Analysis: Equilibria and Kinetics*; Imperial College Press: London.
31. Gregg, S.J.; Sing, K.S.W. (1982) *Adsorption, Surface Area and Porosity*, 2nd Ed.; Academic Press: London.
32. Horváth, G.; Kawazoe, K. (1983) Method for the calculation of effective pore size distribution in molecular sieve carbon. *J. Chem. Eng. Jpn.*, *16*: 470.
33. ABNT, MB-15–Análise Imediata do Carvão, 208–209, 1940 (in Portuguese).
34. Fanning, P.E.; Vannice, M.A. (1993) A drift study of the formation of surface groups on carbon by oxidation. *Carbon*, *31* (5): 721.
35. Toth, J. (1971) State equations of the solid-gas interface layers. *Acta Chim. Acad. Sci. Hung*, *69*: 311.
36. Grande, C.A.; Rodrigues, A. (2008) Electric swing adsorption for CO_2 removal from flue gases. *Int. J. Greenhouse Gas Control*, *2* (2): 194.
37. Grant Glover, T.; Dunne, K.I.; Davis, R.J.; LeVan, M.D. (2008) Carbon-silica composite adsorbent: Characterization and adsorption of light gases. *Microporous Mesoporous Mater.*, *11* (1–3): 1.
38. Vlasov, V.M.; Os'kina, I.A. (2002) Basicity and nucleophilicity of aryl-containing N-anions. *Russ. J. Org. Chem.*, *38* (12): 1705.
39. Morrison, R.; Boyd, R. (1970) Química Orgânica, Fundação Galouste Gulbenkian, 7ª edição, Portugal (in Portuguese).
40. Pevida, C.; Plaza, M.G.; Arias, B.; Fermoso, J.; Rubiera, F.; PIS, J.J. (2008) Surface modification of activated carbons for CO_2 capture. *Appl. Surf. Sci.*, *254* (22): 7165.
41. Wakao, N.; Funazkri, T. (1978) Effect of fluid dispersion coefficients on particle-to-fluid mass transfer coefficients in packed beds: Correlation of Sherwood numbers. *Chem. Eng. Sci.*, *33* (10): 1375.